Systems Actuated by Shape Memory Alloys: Identification and Modeling

Najmeh Keshtkar
Institute of Control Theory
Technische Universität Dresden
Dresden, Germany
najmeh.keshtkar@tu-dresden.de

Johannes Mersch
Institute of Solid-State Electronics
Technische Universität Dresden
Dresden, Germany
johannes.mersch@tu-dresden.de

Konrad Katzer
Institute of Materials Science
Technische Universität Dresden
Dresden, Germany
konrad.katzer1@tu-dresden.de

Felix Lohse
Institute of Textile Technology
Technische Universität Dresden
Dresden, Germany
felix.lohse@tu-dresden.de

Lars Natkowski
Institute of Control Theroy
Technische Universität Dresden
Dresden, Germany
lars.natkowski@mailbox.tu-dresden.de

Gerald Gerlach
Institute of Solid-State Electronics
Technische Universität Dresden
Dresden, Germany
gerald.gerlach@tu-dresden.de

Martina Zimmermann
Institute of Materials Science
Technische Universität Dresden
Dresden, Germany
martina.zimmermann@tu-dresden.de

Chokri Cherif
Institute of Textile Technology
Technische Universität Dresden
Dresden, Germany
chokri.cherif@tu-dresden.de

Klaus Röbenack
Institute of Control Theory
Technische Universität Dresden
Dresden, Germany
klaus.roebenack@tu-dresden.de

***Abstract*—This paper presents the identification of thermal and mechanical parameters of shape memory alloys by using the heat transfer equation and a constitutive model. The identified parameters are then used to describe the mathematical model of a fiber-elastomer composite embedded with shape memory alloys. To verify the validity of the obtained equations, numerical simulations of the SMA temperature and composite bending are carried out and compared with the experimental results.**

I. Introduction

Shape Memory alloys (SMA) are a class of smart materials that possess a unique set of thermomechanical properties, which are based on their two distinct crystallic phases: the low-temperature phase *Martensite* in a twinned and de-twinned state and the high-temperature phase *Austenite* with a periodic cubic crystallic structure. Furthermore, SMAs are capable of phase transitions between the Martensite (M) and the Austenite (A) state via external temperature or stress stimuli. Several material-immanent effects result from this behaviour, the most prominent being the *Shape Memory Effect (SME)*. Here, an initial plastic deformation by external loading in M state can be fully recovered through heating the specimen above its specific transition temperature. Thus, the specimen performs a temperature-induced active deformation that can be utilized to exert forces on external structures, enabling its usage as an actuator. SMAs are well established as actuator materials and have been subject of ample research. The usable power density of SMA is among the highest of all known smart materials [1], enabling a wide range of applications especially in the fields of aerospace [2], [3], robotics [4]–[6] and other areas where weight reduction through functional integration offers performance benefits. A specific field of applications are soft robotics, where flexible rubber-based structures are combined with integrated smart actuators to develop high-performance robotic devices capable of risk-free human-machine interaction [7]–[9].

For designing a system with structurally integrated SMA wires, the characterization of mechanical and thermal properties of the wire as well as the description of the system in terms of constitutive models are of great importance. The most relevant parameters for characterizing SMAs and their thermomechanical behavior for actuation applications are temperature, mechanical stress and strain. Furthermore, the resistance behavior is of importance for electrothermal heating, which is commonly used in most applications with SMAs as actuators. Analytical prediction of the SMAs behavior are mostly investigated through existing constitutive models which include micromechanical, phenomenological and single-crystal-based models [10]. The constitutive models try to describe the SMA behavior as a function of stress, strain and temperature [11].

In this paper, thermo-mechanical properties of a SMA wire is identified through both the heat transfer and constitutive models. Furthermore, an experimental setup is presented which uses integrated SMA wires for actuation of a fiber-elastomer matrix. Simulations are performed to verify the accuracy of the identified parameters and developed equations.

Cite as: N. Keshtkar, J. Mersch, K. Katzer, F. Lohse, L. Natkowski, G. Gerlach, M. Zimmermann, C. Cherif and K. Röbenack, "Systems Actuated by Shape Memory Alloys: Identification and Modeling", *Syst. Theor. Control Comput. J.,* vol. 1, no. 2, pp. 12–20, Dec. 2021.
DOI: 10.52846/stccj.2021.1.2.20

II. Heat Transfer Model

A. Structure of the Model

The first-order heat transfer model of the SMA wire is derived from the balance of energy between natural convection and resistive heating [12]

$$mc_p\dot{T} = -hA_c\left(T - T_\infty\right) + \frac{1}{R}V^2 + m\Delta h\dot{\xi}. \tag{1}$$

In this equation, the left-hand side term is the internal energy which represents the rate of change of temperature and is proportional to mass m and specific heat c_p of the material. The first term of the right-hand side describes the convection heat loss, where h is the heat transfer coefficient, A_c is the area of the wire, and T_∞ is the room temperature. The resistive heating is produced by electrical current passing through the SMA wire and is given by the second term, where R is the resistance of the wire and V is the input voltage. The final term describes the latent heat due to SMA phase transformation, where Δh is the latent heat of transformation and ξ is the martensite fraction. The effect of the latent heat term is shown to be small in comparison to natural convection and resistive heating and can be therefore neglected [12]. Thus, the heat transfer equation reduces to

$$mc_p\dot{T} = -hA_c\left(T - T_\infty\right) + \frac{1}{R}V^2. \tag{2}$$

B. Parameter Identification

The SMA set-up shown in Fig. 1 was used to identify the parameters of the Eq. (2). The SMA wire is a nickel-titanium alloy with $0.3\,mm$ diameter and is clamped on both sides of the frame. The wire is activated by applying an electrical current through it. The current flowing in the wire is measured by a Hall-effect-based current sensor (ACS714). An Optris infrared camera (Xi 400) [13] measures the temperature of the wire. The temperature can be controlled by an Atmel® ATmega328 micro-controller which is mounted on an Arduino® Uno board. MATLAB® R2018b is used to develop the control algorithms.

1) Resistance: The resistance of an SMA wire can be expressed by Ohm's Law

$$R = \frac{V}{I}, \tag{3}$$

where I is the current passing through the wire. By using this linear relationship between voltage and current, the resistance of the SMA sample can be calculated. Resistance measurements are carried out by recording the voltage and current values at regular time intervals using the following method: the voltage was increased $0.25\ V$ every $30\ s$ from 0 up to $6.25\ V$. At the same time, measurements were taken by the current sensor. In every step, the system was allowed to stabilize for $15\ s$ and then the steady-state response was recorded over $15\ s$ and averaged. Then, to compare the resistance during the heating and cooling processes, a decreasing current, from 6.25 to $0\ V$, was applied. The graphical representation of the measurements can be observed in Fig 2.

The experimental results were adjusted to a first-order curve by means of the MATLAB curve fitting toolbox. Then, we considered the resulting curve slopes as the resistance values, which are: $R = 2.6987\ \Omega$ for heating up and $R = 2.6901\ \Omega$ for cooling down.

2) Heat Transfer Coefficient: The unknown heat transfer coefficient was experimentally determined from Eq. (2). By measuring the temperature and voltage at steady state, i.e., when the temperature change rate is zero, the heat coefficient can be found by considering the following relation:

$$h = \frac{V^2}{RA_c(T - T_\infty)}. \tag{4}$$

An experiment was conducted with an increase in the input voltage with steps of $0.25\ V$ and remaining $30\ s$ in each step, allowing the system to reach the steady state and consequently measure the temperature. The relation between measured values of voltage and temperature is shown in Fig 3. The convective heat transfer coefficient was calculated with the MATLAB curve fitting toolbox by adjusting equation 4 to the experimental data. A heat transfer coefficient of $h = 403.26\ W/m^2.K$ was determined.

3) Specific Heat: After identifying the resistance and heat transfer coefficient, the specific heat was determined by the following procedure: first, the voltage was increased from 0 to $2.7\ V$ during $7\ s$, permitting the wire to be heated below the austenite start temperature. The temperature and the input voltage were measured and the derivative of the temperature with respect to time was obtained by the differentiator filter Simulink block. Afterwards, the measured values were adjusted to the following equation:

$$\dot{T} = \frac{1}{c_p}f(T, V), \tag{5}$$

where

$$f(T, V) = \frac{1}{m}(-h_cA_c\left(T - T_\infty\right) + \frac{1}{R}V^2).$$

The specific heat coefficient was found to be $343.2\ J/kg.K$. The plots of measured temperature versus input voltage as well as the derivate of temperature versus $f(T, V)$ are shown in Fig. 4 and 5.

C. Heat Transfer Simulation

The heat transfer equation was simulated numerically using Matlab/Simulink with the Runge–Kutta integration method. The parameters of the equation are presented in Table I. The input of the system is a triangular voltage signal and the output is the temperature. The same input is applied to the experimental setup and the results are shown in Fig. 6.

III. Constitutive model of SMA

A. Constitutive Law

Constitutive models are mathematical representations of the material's mechanical properties which take into account physical concepts and experimental results. The mechanical

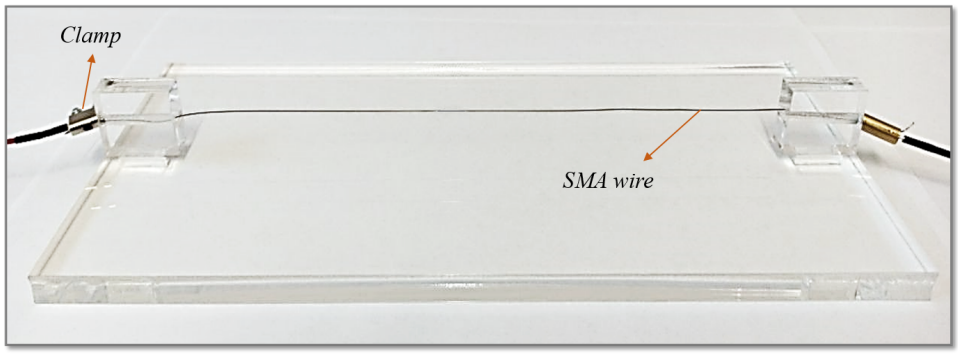

Fig. 1. SMA set-up for identification experiments.

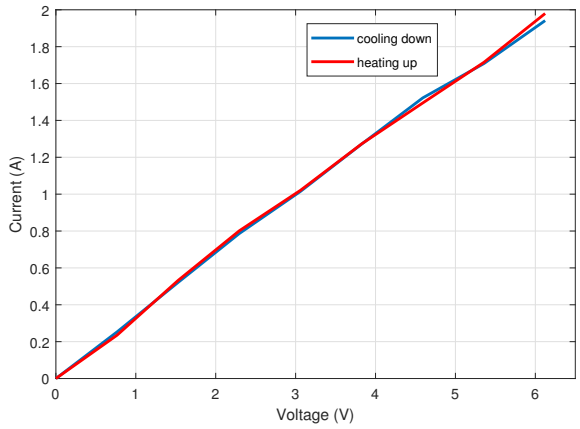

Fig. 2. Measured current versus voltage for resistance identification.

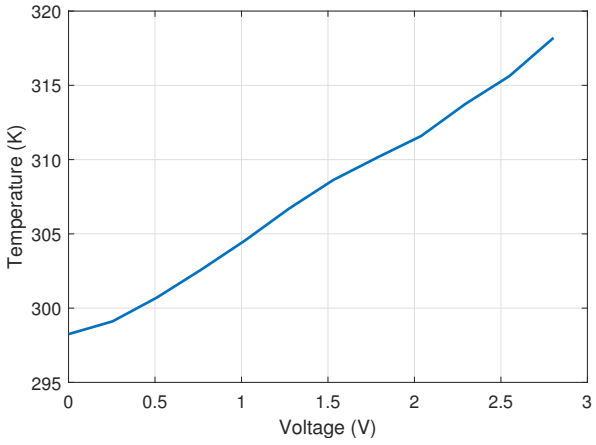

Fig. 3. Measured temperature versus voltage for heat coefficient identification.

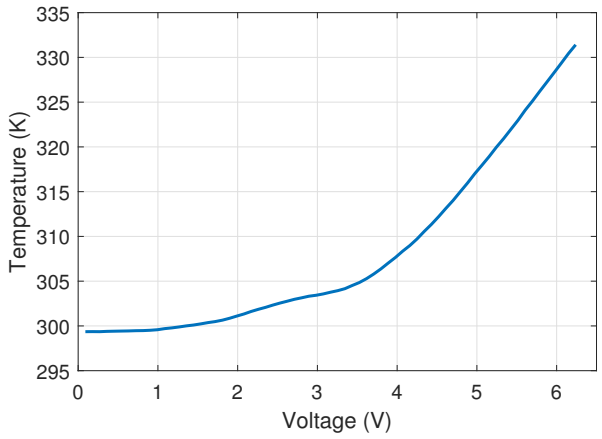

Fig. 4. Measured temperature versus voltage related to specific heat identification.

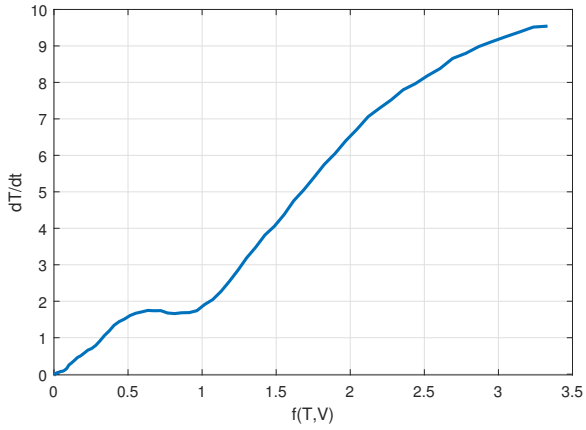

Fig. 5. Derivative of temperature versus f(T,V).

response of the shape memory alloy is characterized by a nonlinear stress–strain relationship associated with other primary variables such as temperature and phase transformation. One of the most widely used constitutive model for SMAs was developed by Liang and Rogers [14]. In this model, the relation between stress σ, strain ε, temperature T and martensite fraction ξ is given by

$$\sigma - \sigma_0 = E(\varepsilon - \varepsilon_0) + \Theta_T(T - T_0) + \Omega(\xi - \xi_0), \quad (6)$$

where σ_0, ε_0 and ξ_0 are the initial conditions of the material. In this equation E is the elasticity module, Θ is the thermal

TABLE I
PARAMETERS OF NITI SMA USED FOR SIMULATION.

Parameter	Description	Value
R	Resitance	$2.6987\ \Omega$
h	Heat transfer coefficient	$403.26\ W/m^2.K$
Cp	Specific heat	$343.2\ J/kg.K$
m	Mass of wire	$0.091\ g$
Ac	Area of wire	$395.84\ mm^2$
T_∞	Ambient temperature	$296.15\ K$

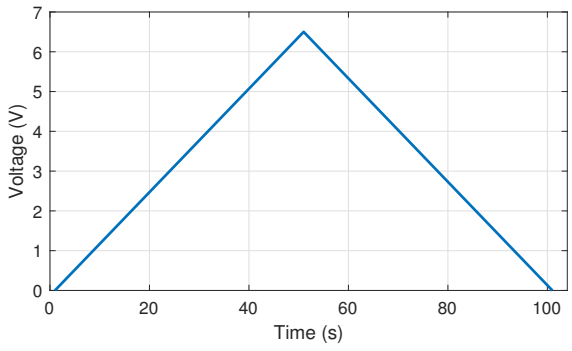

(a)

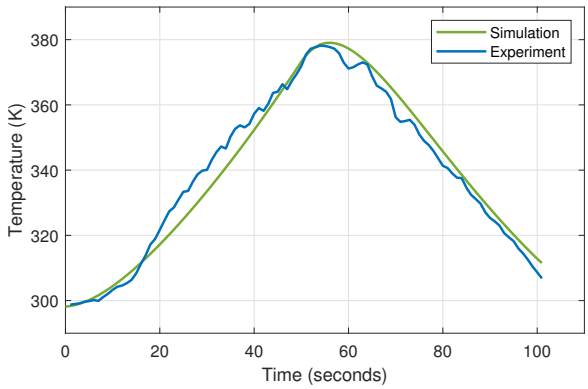

(b)

Fig. 6. Input voltage (a) and resulting temperature response (b).

coefficient of expansion and Ω is the phase transformation coefficient.

B. Parameter Identification

1) Transition temperatures: The phase transition is generally characterized by four distinct temperatures: A_s, A_f, M_s, M_f. They mark the start and end of temperature range for austenite and marteniste phases, respectively. The temperatures are aligned as follows: $A_f > A_s > M_s > M_f$, indicating a hysteresis between $A \rightarrow M$ and $M \rightarrow A$ transformation. A standard procedure for determining the alloy-specific phase transition temperatures of SMA is the differential scale calorimetry (DSC). Here, two crucibles are heated simultaneously in an oven, with one crucible containing sample material and one reference material (usually air). The energy flow of each sample is measured simultaneously during heating and

TABLE II
DSC RESULTS AFTER TWO HEATING CYCLES.

Heat cycle	As	Af	Ms	Mf
1	351.29	371.05	355.49	324.93
2	331.81	353.61	353.39	325.09

compared with each other. When the SMA transforms, the required heat flux differs from the reference crucible, causing a peak in the measurement curve. From these peaks, the transformation temperatures can be derived. In this work, a DSC Q2000 by TA Instruments with a heat rate of 5 K/min and nitrate as purge gas was used. All samples were heated twice from $273.15\ K$ to $453.15\ K$. Fig. 7 shows the resulting graph, from which the temperatures can be determined.

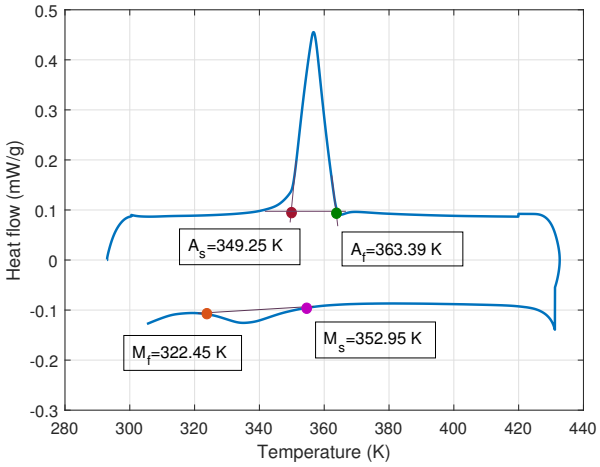

Fig. 7. DSC measurement curve of the NiTi SMA material.

The DSC results confirm the prestretch present within the sample material, indicated by the significantly lower results for A_s and A_f during the second heating cycle (see Table II), while the values for M_s and M_f are nearly identical. After the first cycle, most of the detwinned martensite is recovered. However, with DSC the transition temperatures are obtained under load-free condition and from very small samples. In order to determine values under more application-related conditions, the uniaxial pre-strain free recovery (UPFR) test is being conducted [15]. Here, a specimen is clamped in the Zmart.Pro tensile testing machine from Zwick GmbH & Co. KG and activated by heating while a low constant stress of about $13\,MPa$ ($1\,N$ holding force) is being applied by the machine. Upon activation, the phase change induces a contraction which in turn acts with a force on the clamps, changing the constant value of $1\,N$. The machine then adjusts the clamp position by moving the traverse, so that the measured force is lowered again towards the initial value. The data of the traverse movement can thus be used to measure the contraction of the wire specimen. By plotting the contraction over temperature, both start and end temperature of the phase change can be graphically estimated, corresponding with A_s and A_f. Upon

cooling down below the activation temperature range, M_s and M_f can be obtained in the same manner. Figure 8 shows the graph obtained by testing the NiTi SMA material, yielding a maximum contraction ε_L under nearly load-free-condition of $4.4\,\%$.

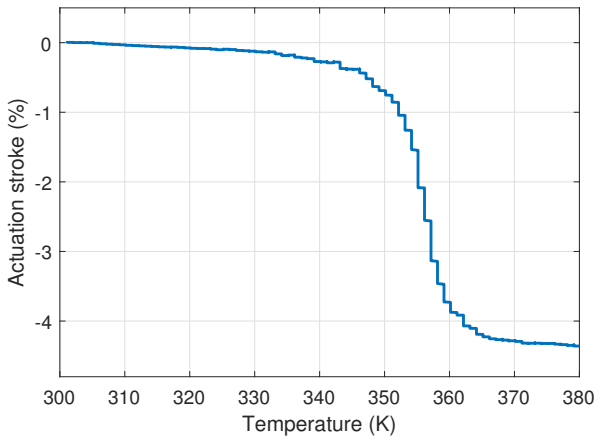

Fig. 8. Experimental curve from a UPFR test on the NiTi SMA wire material.

The UPFR results for the heating phase showed good agreement with the values obtained by DSC measurement, with $350.65 \pm 1.06\ K$ for A_s and $361.35 \pm 1.49\ K$ for A_f. However, with the temperature chamber the cooling down process could not be measured due to unstable cooling behaviour. Furthermore, with SMA wires under external load as is the case in application scenarios, both the maximum actuation stroke and the transition temperatures will digress from the values obtained in near load-free condition.

2) Young's Modulus: The module of elasticity of the SMA is a linear function of the martensite fraction [14]

$$E(\xi) = E_A + \xi(E_M - E_A). \tag{7}$$

For determining the elastic moduli of both M and A phase, tensile tests under constant temperature were conducted, with the test temperature for M phase below M_f and for A phase above A_f. The tensile testing machine with an attached temperature chamber and a $500\ N$ load cell is used. The comparably small load cell and its connecting rod reduce temperature influences on the force measurement. Liquid nitrogen is used as cooling gas. The results of the tensile tests are displayed in Table III.

TABLE III
ELASTIC MODULI OF NITI SMA FOR MARTENSITE AND AUSTENITE STATE.

Parameter	Description	Value in GPa
E_M	Martensitic modulus at $293.15\ K$	22.8 ± 1.2
E_A	Austenitic modulus at $403.15\ K$	55.4 ± 2.5

As shown in Fig. 9, martensite and austenite show different stress-strain behaviour, with martensite displaying a large detwinning area between $0 - 4\ \%$ of strain.

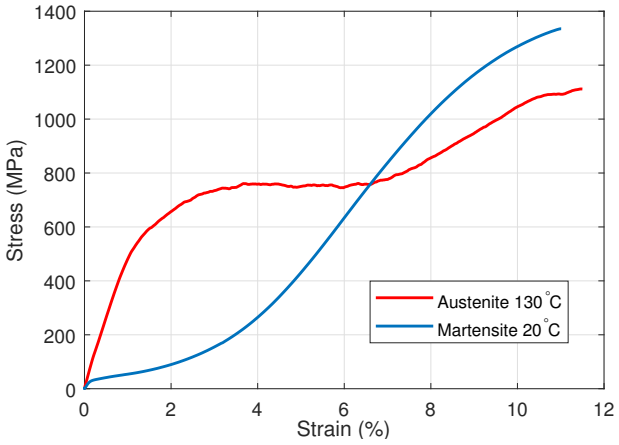

Fig. 9. Stress-strain curves of martensite and austenite.

3) Thermal Expansion Factor: Under some special conditions, the thermal expansion coefficient can be easily calculated from Eq. (6). Prior to phase transformation, the last term of the constitutive equation is reduced to zero as no phase transformation occurs until the austenite start temperature. Furthermore, by fixing the SMA wire from both ends, no change in strain will happen. With the above assumptions the temperature is just a function of the stress, i.e.,

$$\sigma - \sigma_0 = \Theta_T(T - T_0). \tag{8}$$

To satisfy the last assumptions, an experiment with a reference step temperature signal with gradual amplitude increments (stairs signal) was conducted. The step intervals were large enough to permit reaching steady state. During the experiment, force and temperature were measured to calculate the thermal expansion factor. The force was measured using the force transducer of a tensile testing machine and subsequently, the stress was calculated. A proportional-integral control was implemented to follow the reference temperature signal. The temperature-stress plot is shown in Fig. 10. Similar to the experiment outlined in the identification of resistance and heat transfer coefficient, the thermal expansion coefficient was obtained by curve fitting toolbox. This coefficient was determined to be $23.91\,MPa$.

4) Phase Transformation Factor and Martensite Fraction: According to the model developed by Liang and Rogers [14], the phase transformation coefficient is defined as a function of the elasticity module and is given by

$$\Omega = -\varepsilon_L E(\xi). \tag{9}$$

Here, the martensite fraction is a function of stress and temperature. During the martensite to austenite phase transformation, this function is defined by

$$\xi = \frac{1}{2} + \frac{1}{2}\cos[\frac{\pi}{A_f - A_s}(T - A_s - \frac{\sigma}{C_A})], \tag{10}$$

where the parameter C_A is a curve-fitting parameter obtained by experimental tests and indicates the influence of stress on

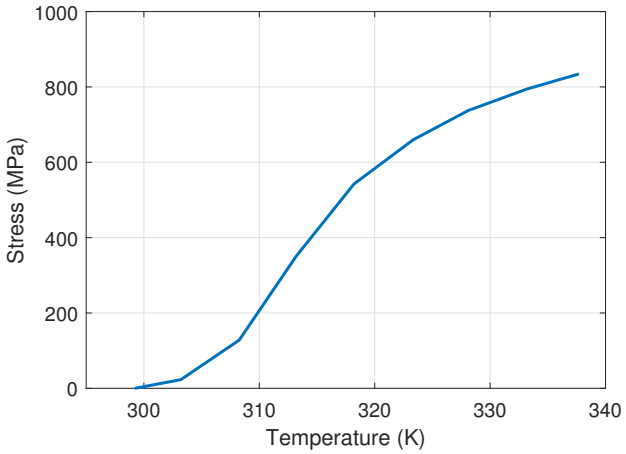

Fig. 10. Measured stress versus temperature for thermal expansion identification.

the transition transformation. On the other hand, the transformation from austenite to marteniste is expressed as

$$\xi = \frac{1}{2} + \frac{1}{2}\cos[\frac{\pi}{M_s - M_f}(T - M_f - \frac{\sigma}{C_M})] \qquad (11)$$

with C_M being a curve fitting parameter. For constant load conditions, the term σ can be omitted from the phase transformation equations.

IV. Example and Results

In this section, the mechanical behavior of a SMA actuated prototype is analyzed with the identified heat transfer and constitutive models. The prototype consists of an integrated fiber-elastomer composite (IFEC) with embedded SMA wires. The wires are covered with a glass fiber-polypropylene sheath. An external elastomer matrix of silicone surrounds the sheath. The schematic of the IFEC as well as its test bench are showed in Fig. 11 and 12. When current is applied, the wires contract and exert a force on the matrix, causing its deflection. To deflect the elastomeric matrix back and forward, four SMA wires are located in the rear and front part of it (two wires per side).

The voltage and current operation ranges of the system are $0 - 10\ V$ and $0 - 3\ A$, respectively. A DC power supply generates the electrical current. To activate the SMA wires, four power channels are required. These channels are switched by a microcontroller (mounted on an Arduino uno board). Two triangulation sensors are used to measure the deflection of the composite and a ACS 712 current sensor to measure the current. The sensor signals are read and processed by Arduino.

A. Composite Bending Model

As the SMA actuators contract upon heating, they generate a force which applies a bending moment M about the composite, leading to its deflection (see Fig. 13). The resulting bending moment is given by

$$M = Pa, \qquad (12)$$

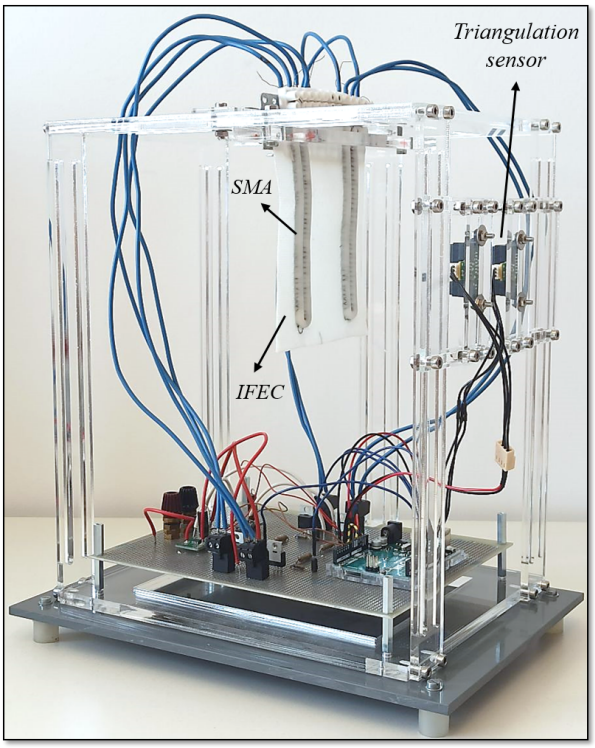

Fig. 11. The test bench for integrated fiber-elastomer composite embedded with SMA wires.

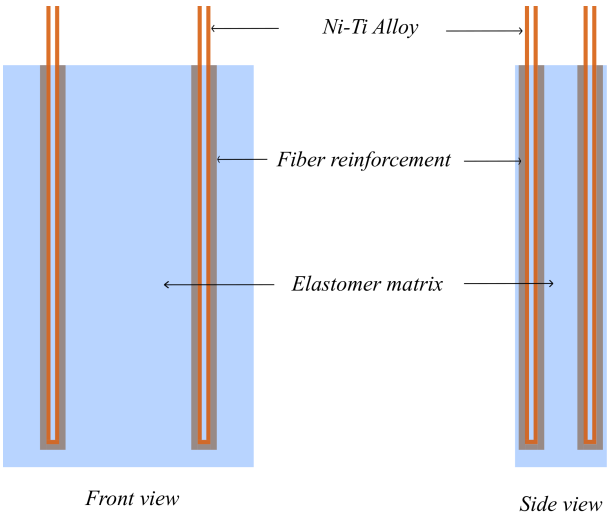

Fig. 12. IFEC specimen Schematic.

where P is the force and a is the distance between the actuators and the composite center-line. Furthermore, the stress in each SMA wire can be calculated by

$$\sigma = \frac{P}{A}, \qquad (13)$$

where A is the cross-section area of the SMA. The bending moment and the curvature angle φ of the composite are related by [16], [17]

$$M = \overline{EI}\frac{d\varphi}{dx}, \qquad (14)$$

where x is the distance from clamping and $\overline{EI}$ indicates the bending stiffness which depends on Young's moduli E of both, composite and SMA wires, as well as their thickness h and width w

$$\overline{EI} = \frac{w_c}{12}\frac{E_c^2 h_c^4 + E_c E h_c h(4h_c^2 + 6h_c h + 4h^2) + h^4 E^2}{E_c h_c + E h}.$$

Here, the composite parameters are indicated by suffix c. The rest of the parameters correspond to the SMA. By replacing Eqs. (12) and (14) in Eq. (13), the stress-deflection relation is expressed as

$$\sigma = \frac{\overline{EI}}{aA}\frac{d\varphi}{dx}. \tag{15}$$

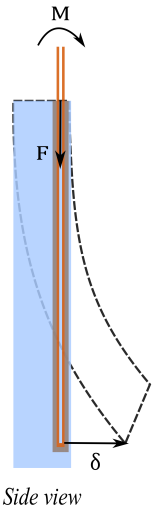

Fig. 13. Composite deflection and generated force and momentum.

On the other hand, the strain-deflection relation can be derived from the two-layer beams theory [16]. By assuming the fiber-SMA sheet as the active layer and the elastomer matrix as the passive layer, the relation between bending curvature and strain is given by [18]

$$\frac{d\varphi}{dx} = \frac{6\varepsilon}{h_c}\frac{\frac{E}{E_c}\cdot\frac{h}{h_c}\frac{h_c+h}{h_c}}{1+(\frac{E}{E_c})^2(\frac{h}{h_c})^4 + \frac{E}{E_c}\frac{h}{h_c}\left[4+6\frac{h}{h_c}+4(\frac{h}{h_c})^2\right]}. \tag{16}$$

By integrating the above equation two times, with respect to x, the deflection δ at position l can be defined as

$$\delta = \frac{6\varepsilon}{h_c}\frac{l^2}{2}\frac{\frac{E}{E_c}\cdot\frac{h}{h_c}\frac{h_c+h}{h_c}}{1+(\frac{E}{E_c})^2(\frac{h}{h_c})^4 + \frac{E}{E_c}\frac{h}{h_c}\left[4+6\frac{h}{h_c}+4(\frac{h}{h_c})^2\right]}. \tag{17}$$

During the experiment, the deflection is measured in a single position along the composite longitude (l is constant). Since the physical parameters of Eq. (17) are also constant, the deflection is just a function of strain.

B. Linearization of the Nonlinear Model

The equations associated with the SMA constitutive model (6), SMA heat transfer (2) and phase transformations (10), (11) along with the composite bending model (17), (15) describe the dynamics of the system. The interaction between these equations is showed in Fig. 14. This model can be used as well for designing shape and deflection controllers. For experimental purposes, the system of equations can be linearized around a point of interest in a typical operation range of the beam, e.g. half of the maximum deflection. The linearized system of equations is expressed as follows

- Constitutive model

$$\begin{aligned}\sigma - \sigma_0 =& a_1(\varepsilon-\varepsilon_0) + \Theta_T(T-T_0)\\ &- \varepsilon_L E_A(\xi-\xi_0) + a_2\xi + a_3,\end{aligned} \tag{18}$$

where

$$\begin{aligned}a_1 &= [E_A + \xi_*(E_M - E_A)],\\ a_2 &= (E_M - E_A)[\varepsilon_L(\xi_0 - 2\xi_*) - \varepsilon_* + \varepsilon_0],\\ a_3 &= (E_M - E_A)\left[\varepsilon_L\xi_*^2 + (\varepsilon_* - \varepsilon_0)\xi_*\right].\end{aligned}$$

- Heat transfer equation

$$mc_p\dot{T} = -hA_c(T - T_\infty) - \frac{V_*}{R}[1+2V]. \tag{19}$$

- Forward phase transformation

$$\xi = b_1(T_* - T + \sigma - \sigma_*) + b_2 \tag{20}$$

with

$$\begin{aligned}b_1 &= \frac{1}{2}\sin\left[\frac{\pi}{A_f - A_s}\left(T_* - A_s - \frac{\sigma_*}{C_A}\right)\right],\\ b_2 &= \frac{1}{2} + \frac{1}{2}\cos\left[\frac{\pi}{A_f - A_s}\left(T_* - A_s - \frac{\sigma_*}{C_A}\right)\right],\end{aligned}$$

- Reverse phase transformation

$$\xi = b_3(T_* - T + \sigma - \sigma_*) + b_4 \tag{21}$$

with

$$\begin{aligned}b_3 &= \frac{1}{2}\sin\left[\frac{\pi}{M_s - M_f}\left(T_* - M_f - \frac{\sigma_*}{C_M}\right)\right],\\ b_4 &= \frac{1}{2} + \frac{1}{2}\cos\left[\frac{\pi}{M_s - M_f}\left(T_* - M_f - \frac{\sigma_*}{C_M}\right)\right].\end{aligned}$$

- Strain deflection equation

$$\varepsilon = \frac{1}{\alpha}\delta, \tag{22}$$

where

$$\alpha = \frac{6}{h_c}\frac{l^2}{2}\frac{\frac{E}{E_c}\cdot\frac{h}{h_c}\frac{h_c+h}{h_c}}{1+(\frac{E}{E_c})^2(\frac{h}{h_c})^4 + \frac{E}{E_c}\frac{h}{h_c}\left[4+6\frac{h}{h_c}+4(\frac{h}{h_c})^2\right]}.$$

- Stress deflection relation

$$\sigma = \beta\delta, \tag{23}$$

where

$$\beta = \frac{2\overline{EI}}{aAl^2}.$$

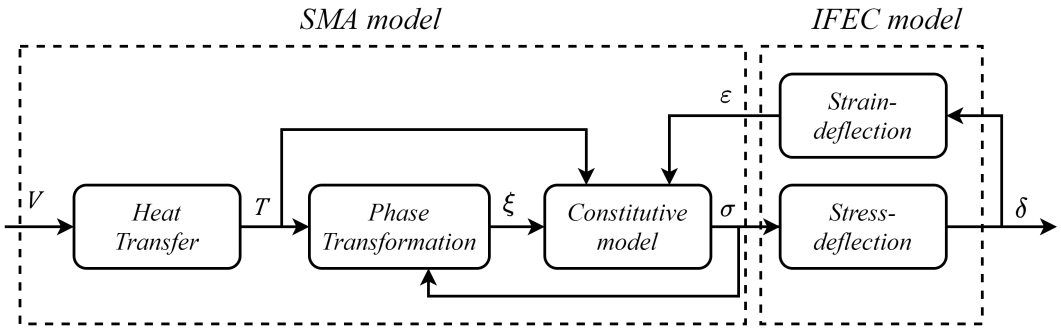

Fig. 14. Block diagram of the IFEC system.

C. Simulation and Experimental Results

The simulation of the composite deflection is performed using Matlab/Simulink. Both triangular and step input functions (Fig. 15) were applied to the system. The corresponding deflections to each input signal are shown in Fig. 16.

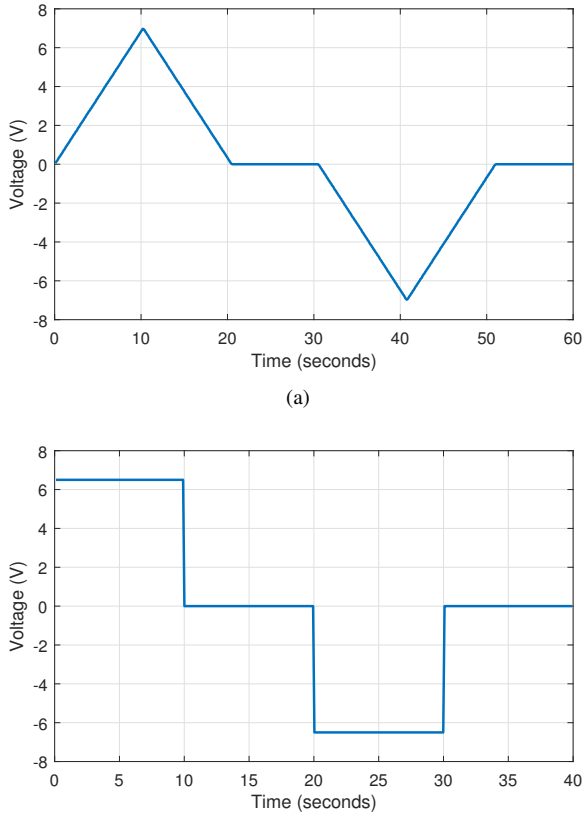

Fig. 15. Input voltage: (a) triangular, (b) step.

Note that in these figures, positive voltage values indicate that the front actuators are activated, meanwhile, negative values represent the activation of the back SMAs. Furthermore, we have included a zero voltage interval in the input functions so that the SMAs will be capable to cool down.

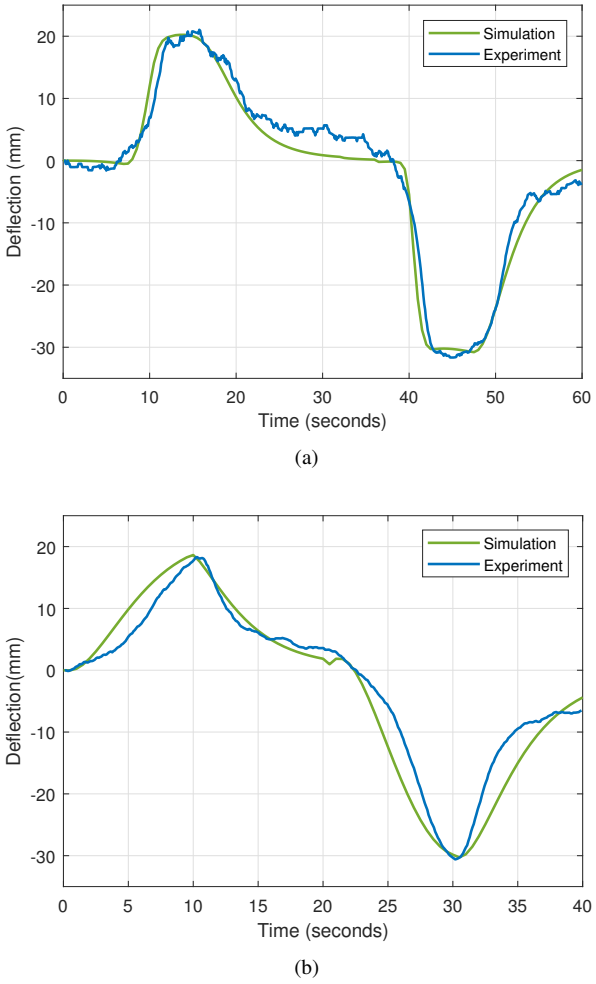

Fig. 16. Output deflection resulting from (a) triangle input and (b) step input.

Due to the manufacturing and assembly processes of our experimental platform, the effective bending stiffness is different for each side of the specimen. Consequently, the deflection of the front and back side is different. As it can be seen from the figures, the experimental results and the numerical simulations are qualitatively similar. The last indicates that the proposed mathematical model, relatively simple, is capable of

describing the SMA deflection. However, it can be observed that the simulation curves reach the zero deflection during the zero voltage interval, nonetheless, this is not the case for the experimental curves. This behavior might be a consequence of the coupling effects between forth and back actuators, such as heat transfer or residual stress, which have not been considered in the mathematical model.

V. Conclusion

In this paper, we have proposed a method to identify thermal, electrical and mechanical SMA wire parameters that are of interest. A heat transfer model as well as a constitutive model are used for the parameters identification. Through these models, unknown coefficients are obtained based on steady-state and step responses in temperature, current, and displacement.

To verify the measured parameters, we used a SMA actuated prototype which consists of a fiber-elastomer composite. The relation between the input voltage and the output deflection of the composite is described by a constitutive model, which considers temperature, phase transformation, stress and strain of the materials. The numerical simulation of the proposed model, with the identified parameters, was carried out in Matlab/Simulink. The numerical deflection results were compared with the experimental measurements. Even though the proposed mathematical model was validated by the experimental results, as a future research it might be worth developing a more complex model which includes the possible coupling effects between the actuators to describe the experimental deflection during the zero voltage intervals more accurately.

Acknowledgment

The DFG research project 380321452/GRK2430 is supported by the Deutsche Forschungsgemeinschaft (DFG, German Research Foundation). The financial support is gratefully acknowledged.

References

[1] D. C. Lagoudas, *Shape memory alloys: modeling and engineering applications*. Springer, 2008.

[2] J. Sun, Q. Guan, Y. Liu, and J. Leng, "Morphing aircraft based on smart materials and structures: A state-of-the-art review," *Journal of Intelligent material systems and structures*, vol. 27, no. 17, pp. 2289–2312, 2016.

[6] X. Huang, K. Kumar, M. K. Jawed, A. Mohammadi Nasab, Z. Ye, W. Shan, and C. Majidi, "Highly dynamic shape memory alloy actuator for fast moving soft robots," *Advanced Materials Technologies*, vol. 4, no. 4, p. 1800540, 2019.

[3] M. Hübler, S. Nissle, M. Gurka, and U. Breuer, "Fiber-reinforced polymers with integrated shape memory alloy actuation: an innovative actuation method for aerodynamic applications," *CEAS Aeronautical Journal*, vol. 7, no. 4, pp. 567–576, 2016.

[4] M. A. Kazemi-Lari, A. D. Dostine, J. Zhang, A. S. Wineman, and J. A. Shaw, "Robotic jellyfish actuated with a shape memory alloy spring," in *Bioinspiration, Biomimetics, and Bioreplication IX*, vol. 10965. International Society for Optics and Photonics, 2019, p. 1096504.

[5] W.-S. Chu, K.-T. Lee, S.-H. Song, M.-W. Han, J.-Y. Lee, H.-S. Kim, M.-S. Kim, Y.-J. Park, K.-J. Cho, and S.-H. Ahn, "Review of biomimetic underwater robots using smart actuators," *International journal of precision engineering and manufacturing*, vol. 13, no. 7, pp. 1281–1292, 2012.

[7] H.-I. Kim, M.-W. Han, S.-H. Song, and S.-H. Ahn, "Soft morphing hand driven by sma tendon wire," *Composites Part B: Engineering*, vol. 105, pp. 138–148, 2016.

[8] J.-H. Lee, Y. S. Chung, and H. Rodrigue, "Long shape memory alloy tendon-based soft robotic actuators and implementation as a soft gripper," *Scientific reports*, vol. 9, no. 1, pp. 1–12, 2019.

[9] J. Hughes, U. Culha, F. Giardina, F. Guenther, A. Rosendo, and F. Iida, "Soft manipulators and grippers: a review," *Frontiers in Robotics and AI*, vol. 3, p. 69, 2016.

[10] H. Talebi, H. Golestanian, M. R. Zakerzadeh, and H. Homaei, "Thermoelectric heat transfer modeling of shape memory alloy actuators," in *The 22st Annual International Conference on Mechanical Engineering-ISME2014, Ahvaz, Iran*, 2014.

[11] H. Sayyaadi, M. R. Zakerzadeh, and H. Salehi, "A comparative analysis of some one-dimensional shape memory alloy constitutive models based on experimental tests," *Scientia Iranica*, vol. 19, no. 2, pp. 249–257, 2012.

[12] O. Heintze and S. Seelecke, "A coupled thermomechanical model for shape memory alloys—from single crystal to polycrystal," *Materials Science and Engineering: A*, vol. 481, pp. 389–394, 2008.

[13] "Infrared camera Optris Xi 400." [Online]. Available: https://www.optris.de/optris-xi-400

[14] C. Liang and C. A. Rogers, "One-dimensional thermomechanical constitutive relations for shape memory materials," *Journal of intelligent material systems and structures*, vol. 8, no. 4, pp. 285–302, 1997.

[15] A. Cadelli, R. Manjeri, F. Sczerzenie, and A. Coda, "Uniaxial prestrain and free recovery (upfr) as a flexible technique for nitinol characterization," *Shape Memory and Superelasticity*, vol. 2, no. 1, pp. 86–94, 2016.

[16] U. Marschner, G. Gerlach, E. Starke, and A. Lenk, "Equivalent circuit models of two-layer flexure beams with excitation by temperature, humidity, pressure, piezoelectric or piezomagnetic interactions," *Journal of Sensors and Sensor Systems*, vol. 3, no. 2, p. 187, 2014.

[17] A. S. Veeramani, G. D. Buckner, S. B. Owen, R. C. Cook, and G. Bolotin, "Modeling the dynamic behavior of a shape memory alloy actuated catheter," *Smart Materials and Structures*, vol. 17, no. 1, p. 015037, 2008.

[18] C. Cherif, R. Hickmann, A. Nocke, M. Schäfer, K. Röbenack, S. Wießner, and G. Gerlach, "Development and testing of controlled adaptive fiber-reinforced elastomer composites," *Textile Research Journal*, vol. 88, no. 3, pp. 345–353, 2018.